



Numerical study of parameters affecting pressure drop of power-law fluid in horizontal annulus for laminar and turbulent flows

Hicham Ferroudji¹ · Ahmed Hadjadj¹ · Ahmed Haddad² · Titus Ntow Ofei³

Received: 8 October 2018 / Accepted: 28 May 2019 / Published online: 1 June 2019
© The Author(s) 2019

Abstract

Efficient hydraulics program of oil and gas wells has a crucial role for the optimization of drilling process. In the present paper, a numerical study of power-law fluid flow through concentric ($E=0.0$) and eccentric annulus ($E=0.3$, $E=0.6$ and $E=0.9$) was performed for both laminar and turbulent flow regimes utilizing a finite volume method. The effects of inner pipe rotation, flow behavior index and diameter ratio on the pressure drop were studied; furthermore, the appearance and development of secondary flow as well as its impact on the pressure drop gradient were evaluated. Results indicated that the increment of the inner pipe rotation from 0 to 400 rpm is found to decrease pressure drop gradient for laminar flow in concentric annulus while a negligible effect is observed for turbulent flow. The beginning of secondary flow formation in the wide region part of the eccentric annulus ($E=0.6$) induces an increase of 9% and a slight increase in pressure drop gradient for laminar and turbulent flow, respectively. On the other hand, the variation of the flow behavior index and diameter ratio from low to high values caused a dramatic increase in the pressure drop. Streamlines in the annulus showed that the secondary flow is mainly induced by eccentricity of the inner pipe where both high values of diameter ratio and low values of flow behavior index tend to prevent the secondary flow to appear.

Keywords Computational fluid dynamics (CFD) · Power-law fluid · Pressure drop · Secondary flow

List of symbols

D_o Diameter of the outer cylinder (m)
 D_i Diameter of the inner cylinder (m)
 D_h Hydraulic diameter (m)
 L_h Length of the hydrodynamic entry (m)
 E Eccentricity of the inner cylinder (–)

κ Diameter ratio (–)
 K Flow consistency index (Pa s^n)
 n Flow behavior index (–)
 u Bulk flow velocity (m/s)
 Re Reynolds number
 ρ Fluid density (kg/m^3)
 $\dot{\gamma}$ Shear rate (s^{-1})

✉ Hicham Ferroudji
hichamf32@gmail.com; ferroudji.h@univ-boumerdes.dz

Ahmed Hadjadj
ahadjad@univ-boumerdes.dz

Ahmed Haddad
a.haddad@crti.dz

Titus Ntow Ofei
titus.ifei@petronas.com.my

- ¹ Laboratory of Petroleum Equipment's Reliability and Materials, Hydrocarbons and Chemistry Faculty, Université M'HAMED BOUGARA, BOUMERDES, Boumerdes, Algeria
- ² Research Center in Industrial Technologies CRTI, BP 64, Route de Dely-Ibrahim, 16033 Chéraga, Algiers, Algeria
- ³ Petroleum Engineering Department, Universiti Teknologi PETRONAS, 32610 Bandar Seri Iskandar, Tronoh, Malaysia

Introduction

The flow of non-Newtonian fluids through annular area has received much attention due to its wide practical applications. This flow is studied to provide solutions for industry challenges, particularly in oil and gas wells drilling like cuttings transport in deviated wells, coiled tubing return flow and cementing. Among problems that can be caused by poor hydraulics design are the insufficient hole cleaning, stuck pipe and lost circulation which causes slow penetration rates (Prassl and Dipl 2003), and produce many costly problems.

Guckes (1975) conducted an earlier study of non-Newtonian fluid in eccentric annuli using a finite difference technique to solve the equations of motion for laminar flow

in bipolar coordinate system. He determined the effects of pressure loss gradient, diameter ratio and eccentricity on the flow rate. Uner et al. (1988) presented the eccentricity as an equivalent slot of variable local annular clearance, where they plotted the flow rate versus pressure loss of power-law and Bingham plastic fluids. However, suitable results are obtained when diameter ratio is high ($\kappa \geq 0.5$). Hacıislamoglu and Langlinais (1990) developed a simple correlation to predict the pressure drop gradient for an eccentric annulus from calculated pressure drop of concentric one. They found that the reduction in the pressure drop in fully eccentric annulus is around 50% less than concentric annulus. McCann et al. (1995) carried out an experimental investigation using flow loop where they found that the pressure drop of power-law fluids decreases significantly in the narrow annuli, while the pressure drop increases with increasing the pipe rotation in turbulent regime. Among known experimental studies of non-Newtonian fluid flow in eccentric annulus with centerbody rotation is that of Nouri and Whitelaw (1994). The authors observed that rotation pipe causes a decrease in pressure drop for low values of Reynolds number; however, the pipe rotation has negligible impact when Reynolds number reaches high values. Likewise, the authors noticed the presence of a counter-rotating swirl flow (also known as secondary flow) in the power-law fluid. The pressure loss changes in non-Newtonian fluids through annulus are attributed to shear-thinning, inertial effects and formation of secondary flows (Ahmed and Miska 2008).

Mitsuishi and Aoyagi (1974) treated experimentally a secondary flow using hydrogen bubbles as tracers, and they noted that the radial velocity component of secondary flow is less than 2% of the axial velocity. However, they did not find such secondary flows for non-Newtonian fluid in a concentric annulus or for Newtonian fluid in an eccentric annulus. Cui and Liu (1995) numerically solved the continuity and momentum equations using bipolar coordinate, and they noticed that the secondary flow area was getting larger as the eccentricity increases. Also they stated that rotation of the inner pipe has not a noticeable effect on the secondary flow. Hussain and Sharif (2000) also performed a numerical study where they concluded that the stagnation in the narrow region of the eccentric annulus tends to intensify the secondary flow.

In the present study, the influence of pipe rotation, diameter ratio (κ) and flow behavior index (n) on the pressure drop for laminar and turbulent flow is evaluated. Moreover, since secondary flow is induced by the second normal stress difference due to the shear in the axial flow and non-symmetric of the cross-sectional geometry (Yue et al. 2008), the effects of eccentricity, flow behavior index and diameter ratio on the appearance and development of secondary flow were studied utilizing a CFD commercial code ANSYS Fluent 17.0.

Moreover, impact of the appearance of secondary flow in the annulus on pressure drop of power-law fluid is discussed.

Mathematical description

To study the pressure drop and secondary flow of non-Newtonian fluid in annular section, the flow is assumed to be fully developed, incompressible, steady and isothermal in both laminar and turbulent regimes.

The continuity and momentum equations that govern the flow are expressed in cylindrical coordinates (r, θ, z), respectively, as (Bird et al. 2002):

$$\frac{1}{r} \frac{\partial(rv_r)}{\partial r} + \frac{1}{r} \frac{\partial(v_\theta)}{\partial \theta} + \frac{\partial(v_z)}{\partial z} = 0 \quad (1)$$

$$\begin{aligned} & \rho \left(\frac{\partial v_r}{\partial t} + v_r \frac{\partial v_r}{\partial r} + \frac{v_\theta}{r} \frac{\partial v_r}{\partial \theta} + v_z \frac{\partial v_r}{\partial z} - \frac{v_\theta^2}{r} \right) \\ &= -\frac{\partial P}{\partial r} - \left(\frac{1}{r} \frac{\partial(r\tau_{rr})}{\partial r} + \frac{1}{r} \frac{\partial(\tau_{\theta r})}{\partial \theta} + \frac{\partial(\tau_{zr})}{\partial z} - \frac{\tau_{\theta\theta}}{r} \right) + \rho g_r \end{aligned} \quad (2)$$

$$\begin{aligned} & \rho \left(\frac{\partial v_\theta}{\partial t} + v_r \frac{\partial v_\theta}{\partial r} + \frac{v_\theta}{r} \frac{\partial v_\theta}{\partial \theta} + v_z \frac{\partial v_\theta}{\partial z} + \frac{v_r v_\theta}{r} \right) \\ &= -\frac{1}{r} \frac{\partial P}{\partial \theta} - \left(\frac{1}{r^2} \frac{\partial(r^2 \tau_{r\theta})}{\partial r} + \frac{1}{r} \frac{\partial(\tau_{\theta\theta})}{\partial \theta} \right. \\ & \quad \left. + \frac{\partial(\tau_{z\theta})}{\partial z} + \frac{\tau_{\theta r} - \tau_{r\theta}}{r} \right) + \rho g_\theta \end{aligned} \quad (3)$$

$$\begin{aligned} & \rho \left(\frac{\partial v_z}{\partial t} + v_r \frac{\partial v_z}{\partial r} + \frac{v_\theta}{r} \frac{\partial v_z}{\partial \theta} + v_z \frac{\partial v_z}{\partial z} \right) \\ &= -\frac{\partial P}{\partial z} - \left(\frac{1}{r} \frac{\partial(r\tau_{rz})}{\partial r} + \frac{1}{r} \frac{\partial(\tau_{\theta z})}{\partial \theta} + \frac{\partial(\tau_{zz})}{\partial z} \right) + \rho g_z \end{aligned} \quad (4)$$

where v_r , v_θ and v_z are the velocity vector components, P is the pressure, ρ is the density and g is the gravity.

For fully developed turbulent flow, the Reynolds stress model (ANSYS FLUENT theory guide 2015) is used to study the effect of the inner pipe rotation, diameter ratio and flow behavior index on pressure drop gradient of power-law fluid in turbulent regime for different eccentricities. The Reynolds stress model is selected among other models (Realizable K-Epsilon, Standard K-Omega and SST K-Omega) based on comparison with the experimental work of McCann et al. (1995) as shown in Fig. 1. Moreover, Sultan et al. (2019) conducted a similar study about the accuracy of different turbulence models, and their results indicate

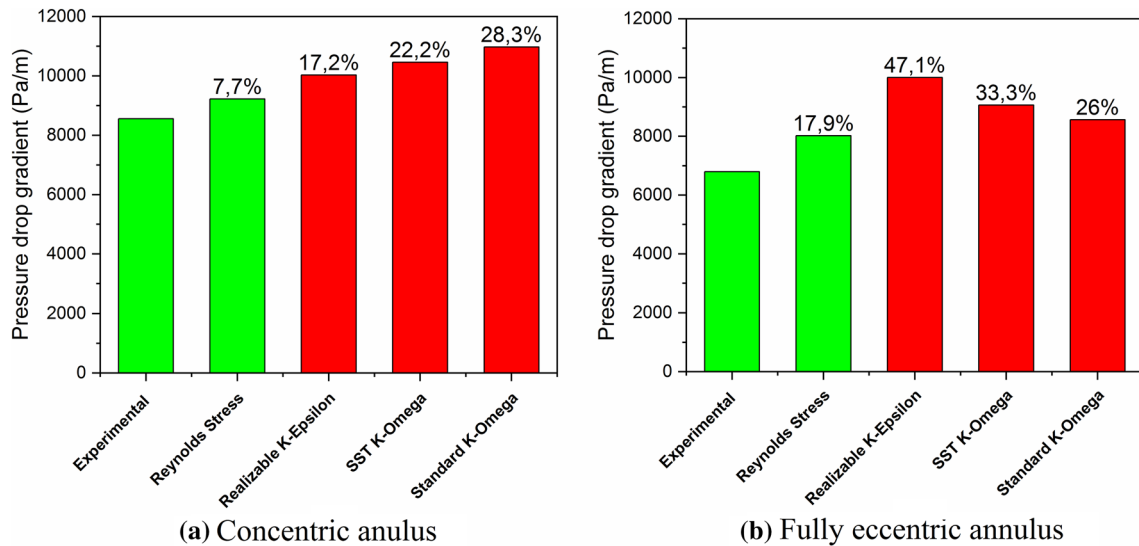


Fig. 1 Comparison of different turbulence models with experimental data of McCann et al. (1995)

that the Reynolds stress model provides accurate results for flow of power-law fluid through concentric and eccentric annulus. For that, the Reynolds stress is utilized to evaluate the influence of the inner pipe rotation, flow behavior index and diameter ratio on the pressure drop gradient of power-law fluid.

The exact transport equation for the Reynolds stress model (RSM) is given as follows:

$$\frac{DR_{ij}}{Dt} = P_{ij} + D_{ij} - \epsilon_{ij} + \vartheta_{ij} + \theta_{ij} \tag{5}$$

where $\frac{DR_{ij}}{Dt}$ is the summation of the changing rate of R_{ij} and transport of R_{ij} by convection, P_{ij} is the production rate of R_{ij} , D_{ij} is the diffusion transport of R_{ij} , ϵ_{ij} is the rate of dissipation, ϑ_{ij} is the pressure–strain correlation term and θ_{ij} is the rotation term.

The diffusion term used in simulation is calculated as follows:

$$D_{T,ij} = \frac{\partial}{\partial x_k} \left(\frac{\mu_t}{\sigma_k} \frac{\partial R_{ij}}{\partial x_k} \right) \tag{6}$$

where $\sigma_k = 0.82$, $\mu_t = C_\mu \left(\frac{k^2}{\epsilon} \right)$ and $C_\mu = 0.09$.

Production rate P_{ij} of R_{ij} or $u'_i u'_j$ can be expressed as:

$$P_{ij} = - \left(\overline{u'_i u'_m} \frac{\partial U_j}{\partial x_m} + \overline{u'_j u'_m} \frac{\partial U_i}{\partial x_m} \right) \tag{7}$$

The pressure–strain term ϑ_{ij} has $\vartheta_{ij,1}$ or slow pressure–strain term also known as the return-to-isotropy term, $\vartheta_{ij,2}$ or rapid pressure–strain term, and $\vartheta_{ij,w}$ as wall reflection term. This term is modeled as:

$$\vartheta_{ij} = \vartheta_{ij,1} + \vartheta_{ij,2} + \vartheta_{ij,w} \tag{8}$$

where

$$\vartheta_{ij,1} = -C_1 \frac{\epsilon}{k} \left[\overline{u'_i u'_j} - \frac{2}{3} \delta_{ij} k \right] \tag{9}$$

$$\vartheta_{ij,2} = -C_2 \left[P_{ij} - \frac{2}{3} \delta_{ij} P \right] \tag{10}$$

where $C_1 = 1.8$ and $C_2 = 0.6$.

The wall reflection term $\vartheta_{ij,w}$ is responsible for the normal stresses distribution near the wall. This term is determined as follows:

$$\begin{aligned} \vartheta_{ij,w} \equiv & C'_1 \frac{\epsilon}{k} \left(\overline{u'_k u'_m} n_k n_m \delta_{ij} - \frac{3}{2} \overline{u'_i u'_k} n_j n_k - \frac{3}{2} \overline{u'_j u'_k} n_i n_k \right) \frac{C_l k^{\frac{3}{2}}}{\epsilon d} \\ & + C'_2 \left(\overline{\vartheta_{km,2} n_k n_m} \delta_{ij} - \frac{3}{2} \overline{\vartheta_{ik,2} n_j n_k} - \frac{3}{2} \overline{\vartheta_{jk,2} n_i n_k} \right) \frac{C_l k^{\frac{3}{2}}}{\epsilon d} \end{aligned} \tag{11}$$

where $C'_1 = 0.5$, $C'_2 = 0.3$, n_k is the horizontal component of the component normal to the wall, d is the shortest distance to the wall and $C_l = \frac{C_\mu^{3/4}}{k}$, where $C_\mu = 0.09$ and k is the von Kármán constant ($=0.4187$).

The dissipation rate ϵ_{ij} or the destruction rate of R_{ij} is modeled as:

$$\epsilon_{ij} = \frac{2}{3} \delta_{ij} \epsilon \tag{12}$$

where

$$\epsilon = 2\nu \overline{s'_{ij} \cdot s'_{ij}} \tag{13}$$

and s'_{ij} = fluctuating deformation rate.

Table 1 Fluid and geometry characteristics

Non-Newtonian fluid	Fluid and geometry characteristics			
	K (Pa s ⁿ)	n (–)	D_o (mm)	D_i (mm)
Ostwald–de Waele power law	0.25	0.61	38.1	19.05

Rotation term is expressed as:

$$\theta_{ij} = -\omega_k (R_{jm} e_{ikm} + R_{im} e_{jkm}) \quad (14)$$

where ω_k is the rotation vector, e_{ikm} = alternating symbol, + 1, – 1 or 0 depending on i, j and k .

Simulation methodology

Physical model

The flow of non-Newtonian fluid is bounded by two horizontal cylinders, where the outer cylinder is fixed and inner one rotates to simulate the mud pattern in horizontal borehole. In this model, the fluid flows through concentric and eccentric annulus $E=0.3$, $E=0.6$ and $E=0.9$ in which the eccentricity is defined as:

$$E = \frac{2e}{D_o - D_i} \quad (15)$$

where e is the distance between centers.

The fluid characteristics and geometry dimensions are listed in Table 1.

To determine the fluid flow regime, Reynolds number is calculated using the relationship of Madlener et al. (2009)

$$Re = \frac{\rho D_h^n u^{2-n}}{K \left(\frac{3n+1}{4n} \right)^n 8^{n-1}} \quad (16)$$

where u is the bulk flow velocity and D_h is the hydraulic diameter which is calculated as:

$$D_h = D_o - D_i \quad (17)$$

The length of the cylinders is selected to be longer than hydrodynamic entry length to prevent the entrance effects, where the hydrodynamic entry length is given as Yunus and Cimbala (2006)

$$L_{h,laminar} = 0.05(D_o - D_i)Re \quad (18)$$

$$L_{h,turbulent} = 1.359(D_o - D_i)Re^{1/4} \quad (19)$$

Table 2 summarizes the range of different parameters studied in the present numerical study.

Table 2 Range of the numerical study parameters

Parameters of the numerical study	Range of the parameters
Fluid velocity (m/s)	0.2–2
Re number (–)	94–701,811
Inner pipe rotation (rpm)	0–400
Eccentricity (–)	0–0.9
Flow behavior index (Pa s ⁿ)	0.1–0.9
Diameter ratio (–)	0.3–0.9

CFD model

Default standard wall functions are generally applicable if the first cell center adjacent to the wall has a (y^+) value larger than 30 (ANSYS FLUENT theory guide 2015); for that, the dimensionless wall distance (y^+) is checked during mesh generation in consideration of the requirement of (y^+) and maintained above the value of 40. The value of (y^+) is calculated using the following relationship:

$$y^+ = \frac{y}{\mu} \sqrt{\rho \tau_w} \quad (20)$$

where τ_w is the wall shear stress, ρ the fluid density, y the distance from the wall and μ the molecular viscosity.

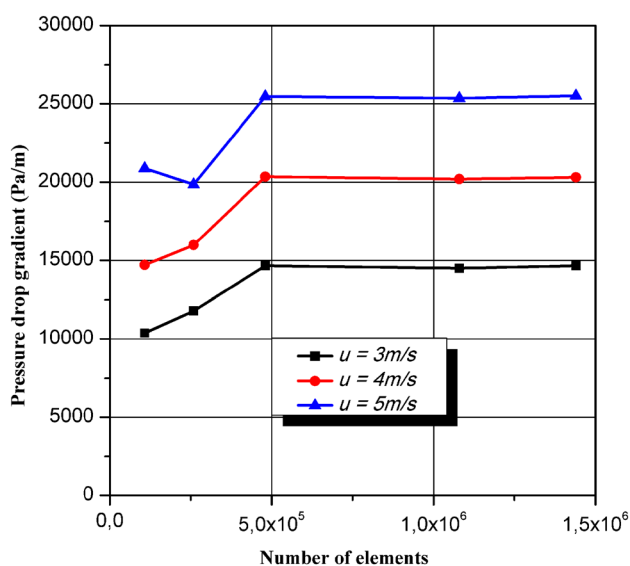
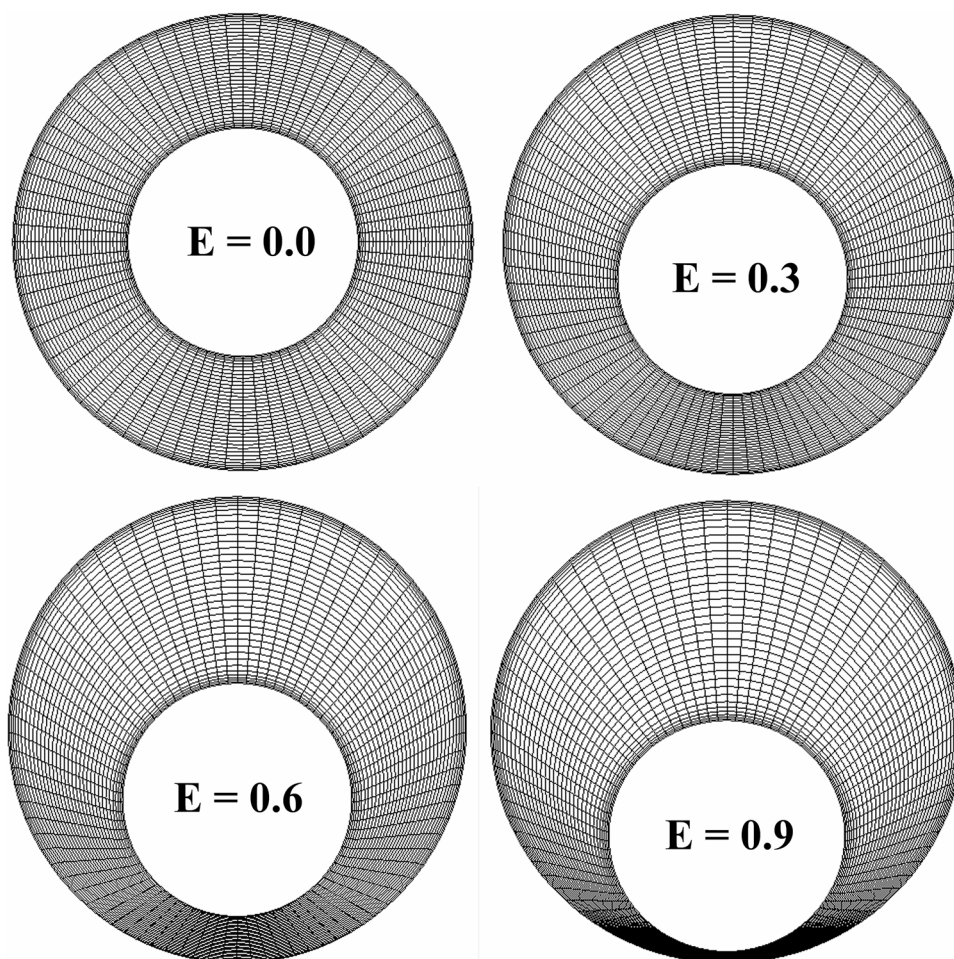
To attain the solution, the numerical study is performed with 1,120,000 hexahedral elements (35 radial divisions, 80 circumferential divisions and 400 axial divisions) in which the near walls are refined to obtain an accurate solution of the streamline function in these regions (Fig. 2). For that, a CFD software ANSYS Fluent 17.0 is used to solve Navier–Stokes (NS) equations based on finite volume method, as well as $k-\epsilon$ equations for turbulent regime allowing calculation of the turbulent viscosity.

The numerical solution of the governing equations is based on pressure–velocity coupling, in which the algorithm SIMPLE was used. For the discretization of pressure and momentum equations, PRESTO and second-order upwind are used, respectively.

Residuals of an iterative calculation are considered as convergence criteria, and the accurate results are obtained by making residuals as small as possible. For the convergence criteria of the present work, a value of 10^{-4} is selected.

Validation model

Figure 3 shows that the results provided by numerical calculations are independent of the mesh model used, where critical conditions were adopted (Reynolds number Re from 5070 to 10,312 and $E=0.9$) in the grid independence study.

Fig. 2 Cross section of concentric and eccentric annulus**Fig. 3** Mesh independence study

The predicted results of pressure drop versus drill pipe rotation from 0 to 400 rpm using CFD are compared with different previous experimental works from the literature (McCann et al. 1995, Vieira Neto et al. 2014 and Ahmed and Miska 2008) as shown in Fig. 4. Moreover, the rheological parameters and geometry characteristics of the experimental studies are summarized in Table 3. In Fig. 4a, a slight deviation is stated between the experimental and simulation results where the mean error is estimated at 5.5% and 3.8% for 0.181 m/s and 0.362 m/s fluid velocity, respectively. Similarly, the calculated pressure drop slightly overpredicted the experimental results by 11.5% and 13.1% for XG 0.2% and CMC 0.2% fluids, respectively, as shown in Fig. 4b; furthermore, the simulation and experimental results are in good agreement as shown in Fig. 4c, in which the mean percentage error is 1.87% and 6.08% for 1.03 m/s and 0.44 m/s fluid bulk velocity, respectively. The comparison proves the ability of CFD model to provide accurate results.

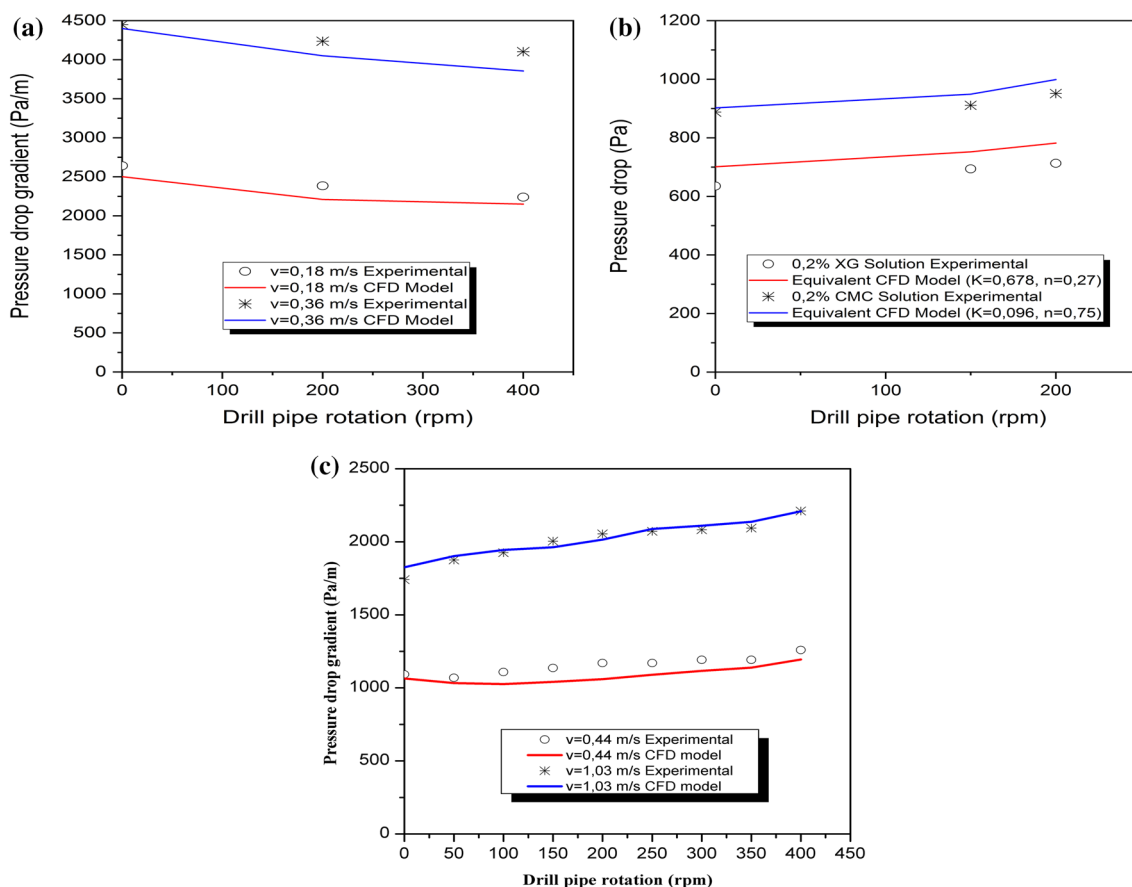


Fig. 4 Comparison of simulated and the experimental data: **a** power-law fluid through concentric annulus (McCann et al. 1995), **b** power-law fluid through eccentric annulus

Table 3 Fluid and geometry characteristics

Experimental works	K (Pa s ⁿ)	n (-)	Inner pipe rotation (rpm)	κ (D_i/D_o)	E (-)
McCann et al. (1995)	0.095	0.65	0–800	0.71, 0.83 and 0.9	0
Vieira Neto et al. (2014)	0.67	0.27	0–300	0.48	0 and 0.75
	0.09	0.75	0–300	0.48	0 and 0.75
Ahmed and Miska	0.25	0.61	0–400	0.5 and 0.67	0.1

Results and discussion

Effects of pipe rotation, flow behavior index and diameter ratio on pressure drop gradient

Figure 5 shows a reduction in the pressure drop gradient in the concentric annulus ($E = 0.0$) for laminar flow regime, in which the reduction is around 10% when the pipe rotation increases from 50 to 400 rpm. This reduction is due to the shear-thinning effect of power-law fluids. However, pipe rotation causes an increase of 9% of pressure drop gradient in the annulus of $E = 0.6$. This increase could be

attributed to the beginning of the secondary flow formation where the flow in the wide region of annulus begins to form a counter-rotating swirl (Fig. 10). A negligible effect of the inner pipe rotation on pressure drop loss gradient is, however, observed for the eccentric annulus of $E = 0.3$ and $E = 0.9$.

For turbulent regime, a negligible influence is noticed of the drill pipe rotation on pressure drop gradient for concentric and eccentric annulus, except for annulus of $E = 0.6$, where a slight increase was noticed with increasing the drill pipe rotation as shown in Fig. 6.

Figures 7 and 8 depict an exponential increase in pressure drop gradient when the value of flow behavior index

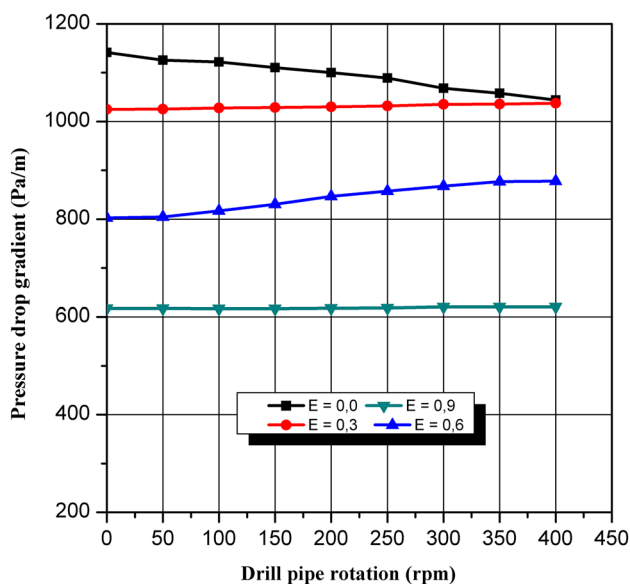


Fig. 5 Effect of the pipe rotation on pressure drop gradient in concentric and eccentric annulus for laminar regime ($Re=94$, $u = 0.2$ m/s, $\kappa = 0.5$, $n = 0.61$)

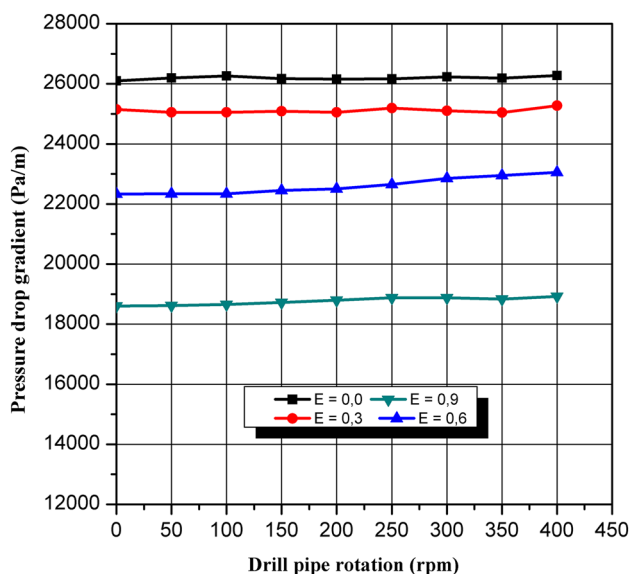


Fig. 6 Effect of the pipe rotation on pressure drop gradient in concentric and eccentric annulus for turbulent regime ($Re=6100$, $u = 2$ m/s, $\kappa = 0.5$, $n = 0.61$)

increases for a constant diameter ratio, where power-law fluid is less affected by shear-thinning effect as this behavior gets closer to Newtonian fluid in both laminar and turbulent regimes.

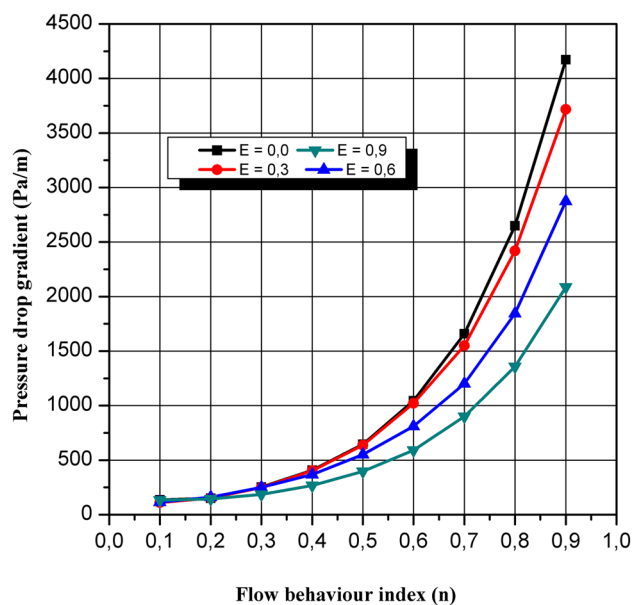


Fig. 7 Effect of the flow behavior index on pressure drop gradient in concentric and eccentric annulus for laminar regime (Re =from 28 to 870, $u = 0.2$ m/s, $\kappa = 0.5$, $\omega = 200$ rpm)

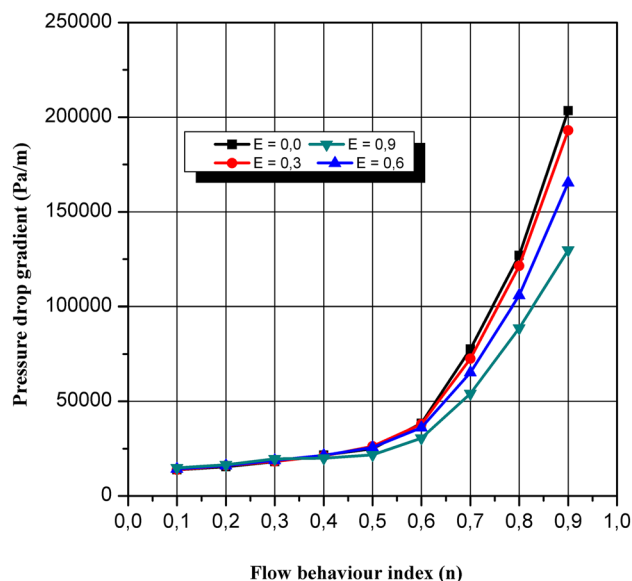


Fig. 8 Effect of the flow behavior index on pressure drop gradient in concentric and eccentric annulus for turbulent regime (Re =from 3200 to 701811, $u = 2$ m/s, $\kappa = 0.5$, $\omega = 200$ rpm)

As illustrated in Figs. 9 and 10, the pressure drop gradient increases gradually for low values of diameter ratio, whereas this increase becomes significant when diameter ratio reaches 0.6, particularly from $\kappa = 0.8$ to $\kappa = 0.9$ where the pressure drop increased sharply. This observed phenomenon is related to narrow annulus of oil and gas wells such as casing-while-drilling, where extra caution is

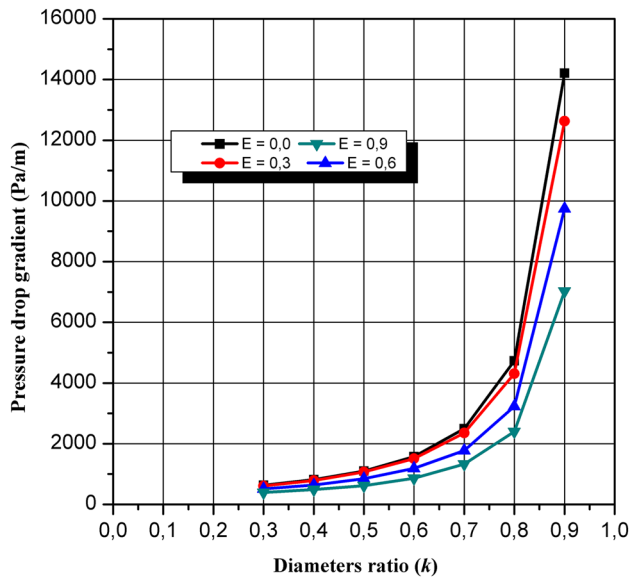


Fig. 9 Effect of diameter ratio on pressure drop gradient in concentric and eccentric annulus for laminar regime (Re =from 35 to 115, $u = 0.2$ m/s, $n = 0.61$, $\omega = 200$ rpm)

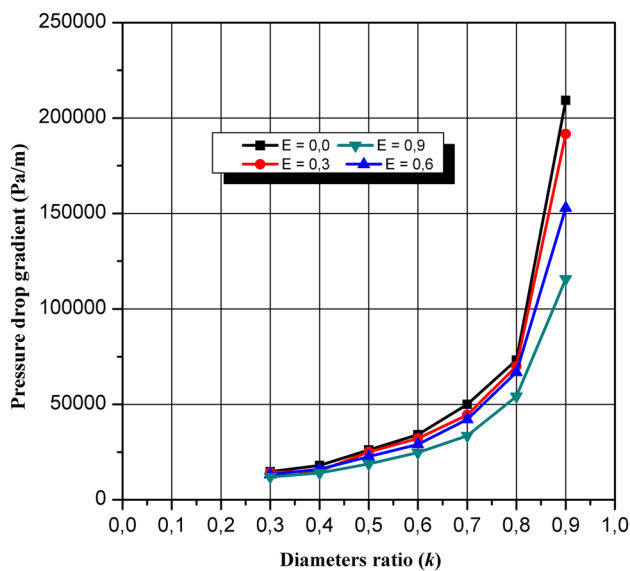


Fig. 10 Effect of diameter ratio on pressure drop gradient in concentric and eccentric annulus for turbulent regime (Re =from 2531 to 7428, $u = 2$ m/s, $n = 0.61$, $\omega = 200$ rpm)

required preventing formation fracture due to the occurrence of high equivalent circulating density (ECD) during drilling operation.

For all parameters studied in the present study, pressure drop gradient diminishes as the eccentricity increases.

Effects of eccentricity, flow behavior index and diameter ratio on secondary flow

As shown in Fig. 12, for the eccentric annulus ($E=0.3$) there was no formation of secondary flow, however, for the annulus of $E=0.6$, a counter-rotating swirl begins to appear in the wide region part of the annulus for a flow behavior index from 0.4 ($n \geq 0.4$) where the flow rotates in the opposite direction of the inner pipe. The appearance of secondary flow formation in this annulus could explain again the increase of pressure drop gradient of the eccentric annulus of $E=0.6$ in Fig. 4.

Conversely, a fully developed counter-rotating swirl was observed for the annulus of $E=0.9$ in which small difference in the second normal stress caused by low values of the flow behavior index tends to prevent the secondary flow to appear.

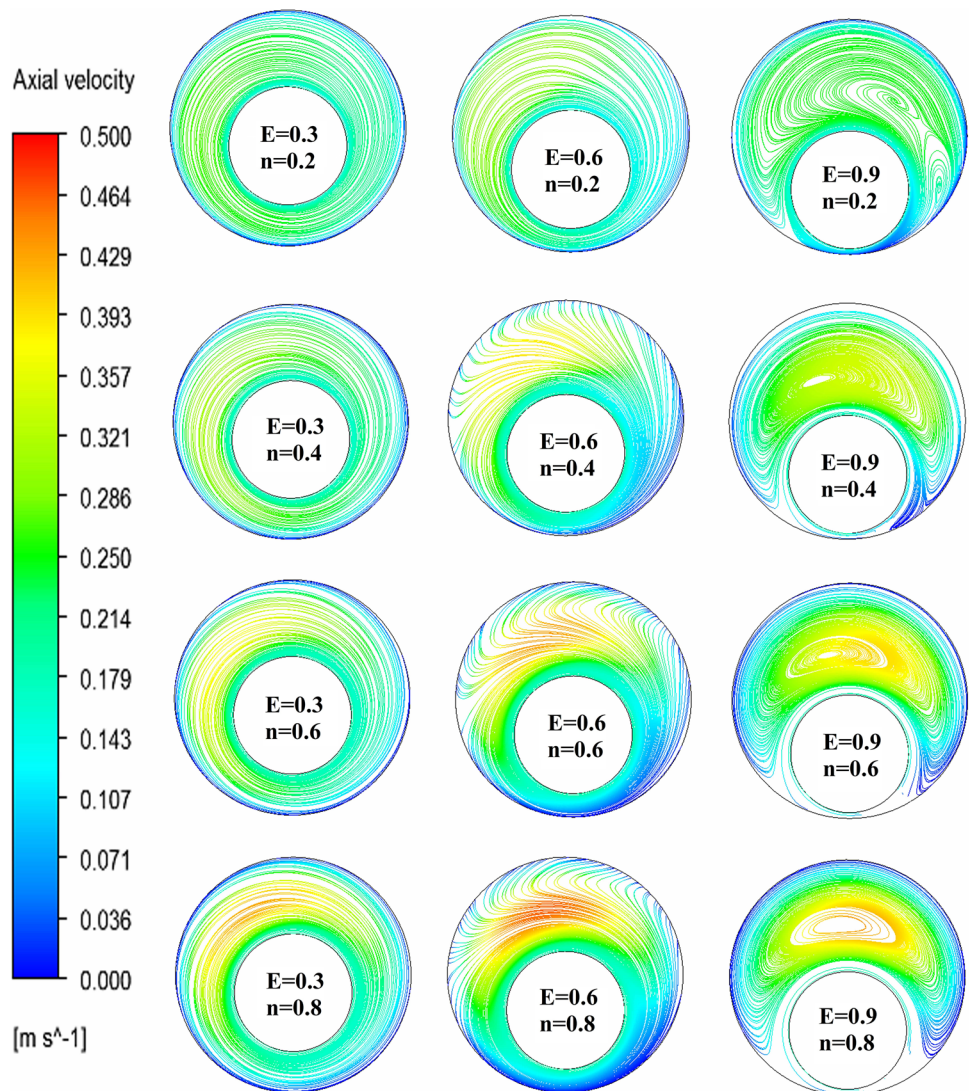
Figure 11 exhibits that no secondary flow occurs in the annulus of $E=0.3$ for all range of diameter ratio. For the eccentric annulus of $E=0.6$, the area of secondary flow decreases with increasing diameter ratio up to $\kappa=0.7$ where the secondary flow was disappeared; however, for the eccentric annulus of $E=0.9$ a developed secondary flow is observed for all diameter ratios.

Since cuttings are transported in the wide region of eccentric annulus which is characterized by high velocity and viscosity, the tendency of the inner pipe rotation to move the flat region of power-law velocity profile from the wide region part to the narrow region part of the annulus ($E=0.3$ and $E=0.6$) could improve hole cleaning efficiency by preventing cuttings bed formation. A negligible effect of the inner pipe rotation on the flat region is observed for the eccentric annulus of $E=0.9$ for high values of flow behavior index and low of diameter ratios, as shown in Figs. 10 and 11, respectively.

It can be concluded from the comparison between Figs. 5 and 12 that beginning of formation of the secondary flow causes the increase in pressure drop gradient for the eccentric annulus of $E=0.6$; however, the fully developed secondary flow in the eccentric annulus of $E=0.9$ did not have a significant effect on pressure drop gradient.

For all parameters affecting formation and development of the secondary flow, the Reynolds stress of the flow has low values in which the developed secondary flow is found almost symmetric in the annulus. Same trend was stated in the work of Escudier et al. (2002)

Fig. 11 Effect of flow behavior index on the streamlines and axial velocity for eccentric annulus $E=0.3$, $E=0.6$ and $E=0.9$ ($u=0.2$)

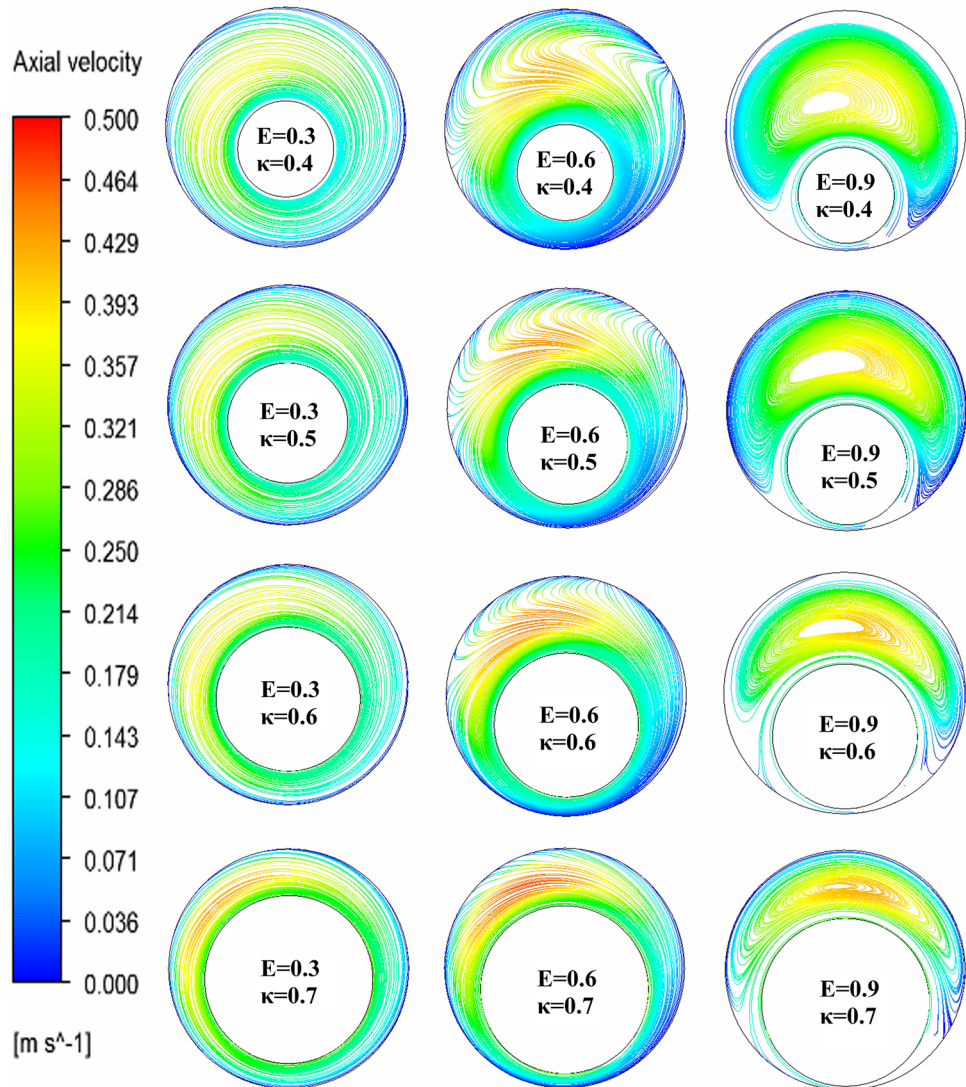


Conclusions

The following conclusions were reported from this study:

- For laminar flow regime, the rotation of the inner pipe causes a reduction in pressure drop gradient of power-law fluid in concentric annulus; however, a negligible effect is observed for eccentric annulus except for annulus ($E=0.6$).
- There was no a significant effect of the inner pipe cylinder rotation on the pressure drop gradient in turbulent flow regime.
- As power-law fluid index gets closer to Newtonian behavior, the pressure drop gradient increases exponentially for a constant diameter ratio.
- High values of diameter ratio cause a significant increase in the pressure drop gradient, particularly from $\kappa=0.8$ to $\kappa=0.9$ where the pressure drop gradient is increased dramatically.
- Secondary flow of power-law fluid is mainly caused by eccentricity of the inner pipe cylinder where both high values of diameter ratio and low values of flow behavior index tend to prevent the secondary flow to appear.
- Flat region of velocity profile of power-law fluids in the wide region of eccentric annulus is less affected by the inner pipe rotation when the eccentricity reaches high values.
- Beginning formation of the secondary flow in the wide region of eccentric annulus of $E=0.6$ induces the

Fig. 12 Effect of diameter ratio on the streamlines and axial velocity for eccentric annulus $E=0.3$, $E=0.6$ and $E=0.9$ ($u=0.2$)



increase in pressure drop gradient; however, a slight effect is observed for the annulus of $E=0.9$ where the secondary flow was fully developed.

Open Access This article is distributed under the terms of the Creative Commons Attribution 4.0 International License (<http://creativecommons.org/licenses/by/4.0/>), which permits unrestricted use, distribution, and reproduction in any medium, provided you give appropriate credit to the original author(s) and the source, provide a link to the Creative Commons license, and indicate if changes were made.

References

- Ahmed RM, Miska SZ (2008) Experimental Study and Modeling of Yield Power-Law Fluid Flow in Annuli With Drillpipe Rotation. InL IADC/SPE Drilling Conference. Society of Petroleum Engineers
- Bird R, Stewart WE, Lightfoot EN (2002) Transport phenomena. Wiley, Hoboken
- Cui HQ, Liu XS (1995) Research on helical flow of non-Newtonian fluids in eccentric annuli. In: International meeting on petroleum engineering. Society of petroleum engineers
- Escudier MP, Oliveira PJ, Pinho FT (2002) Fully developed laminar flow of purely viscous non-Newtonian liquids through annuli, including the effects of eccentricity and inner-cylinder rotation. *Int J Heat Fluid Flow* 23(1):52–73
- Fluent A (2015) Theory Guide Release 16.1 Ansys Inc
- Guckes TL (1975) Laminar flow of non-Newtonian fluids in an eccentric annulus. *J Eng Ind* 97(2):498–506
- Haciislamoglu M, Langlinais J (1990) Non-Newtonian flow in eccentric annuli. *J Energy Res Technol* 112(3):163–169
- Hussain QE, Sharif MAR (2000) Numerical modeling of helical flow of pseudoplastic fluids. *Numerical Heat Transfer Part A Appl* 38(3):225–241
- Madlener K, Frey B, Ciezki HK (2009) Generalized Reynolds number for non-Newtonian fluids. *Prog Propuls Phys* 1:237–250
- McCann RC, Quigley MS, Zamora M, Slater KS (1995) Effects of high-speed pipe rotation on pressures in narrow annuli. *SPE Drill Complet* 10(02):96–103

- Mitsuishi N, Aoyagi Y (1974) Non-Newtonian fluid flow in an eccentric annulus. *J Chem Eng Jpn* 6(5):402–408
- Nouri JM, Whitelaw JH (1994) Flow of Newtonian and non-Newtonian fluids in a concentric annulus with rotation of the inner cylinder. *J Fluids Eng* 116(4):821–827
- Prassl WF, Dipl L (2003) *Drilling Engineering* Dept of Petroleum Engineering. Curtin University of Technology, Kensington
- Sultan RA, Rahman MA, Rushd S, Zendejboudi S, Kelessidis VC (2019) CFD Analysis of pressure losses and deposition velocities in Horizontal Annuli. *Int J Chem Eng* 2019:7068989. <https://doi.org/10.1155/2019/7068989>
- Uner D, Ozgen C, Tosun I (1988) An approximate solution for non-Newtonian flow in eccentric annuli. *Ind Eng Chem Res* 27(4):698–701
- Vieira Neto JL, Martins AL, Ataíde CH, Barrozo MAS (2014) The effect of the inner cylinder rotation on the fluid dynamics of non-Newtonian fluids in concentric and eccentric annuli. *Braz J Chem Eng* 31(4):829–838
- Yue P, Dooley J, Feng JJ (2008) A general criterion for viscoelastic secondary flow in pipes of noncircular cross section. *J Rheol* 52(1):315–332
- Yunus AC, Cimbala JM (2006) *Fluid mechanics fundamentals and applications*, International edn. McGraw Hill Publication, New York
- Publisher's Note** Springer Nature remains neutral with regard to jurisdictional claims in published maps and institutional affiliations.